

Suzaku Observation of Be/X-ray Binary Pulsar EXO 2030+375

Sachindra Naik and Gaurava K. Jaisawal

Astronomy and Astrophysics Division, Physical Research Laboratory, Ahmedabad, India ;
snaik@prl.res.in

Received ...; accepted ...

Abstract In this paper we study the timing and spectral properties of Be/X-ray binary pulsar EXO 2030+375 using a *Suzaku* observation on 2012 May 23, during a less intense Type I outburst. Pulsations were clearly detected in the X-ray light curves at a barycentric period of 41.2852 s which suggests that the pulsar is spinning-up. The pulse profiles were found to be peculiar e.g. unlike that obtained from the earlier *Suzaku* observation on 2007 May 14. A single-peaked narrow profile at soft X-rays (0.5-10 keV range) changed to a double-peaked broad profile in 12-55 keV energy range and again reverted back to a smooth single-peaked profile at hard X-rays (55-70 keV range). The 1.0-100.0 keV broad-band spectrum of the pulsar was found to be well described by three continuum models such as (i) a partial covering high energy cut-off power-law model, (ii) a partially absorbed power-law with high-energy exponential rolloff and (iii) a partial covering Negative and Positive power law with EXponential (NPEX) continuum model. Unlike earlier *Suzaku* observation during which several low energy emission lines were detected, a weak and narrow Iron K_{α} emission line at 6.4 keV was only present in the pulsar spectrum during the 2012 May outburst. Non-detection of any absorption like feature in 1-100 keV energy range supports the claim of absence of cyclotron resonance scattering feature in EXO 2030+375 from earlier *Suzaku* observation. Pulse-phase resolved spectroscopy revealed the presence of additional dense matter causing the absence of second peak from the soft X-ray pulse profiles. The details of the results are described in the paper.

Key words: pulsars: individual (EXO 2030+375); stars: neutron; X-rays: stars

1 INTRODUCTION

X-ray Binaries are known to be strong X-ray emitters and appear as the brightest X-ray sources in the sky. Depending on the mass of the optical companion, X-ray binaries are classified as low mass X-ray binaries (LMXBs) and high mass X-ray binaries (HMXBs). Based on the type of optical companion, the HMXBs are further classified as Be/X-ray binaries (largest subclass of HMXBs) and supergiant X-ray binaries. Though evolutionary model calculations show that binary systems with white dwarf and Be star or black hole and Be star should also exist, observational evidence on the existence of such binary systems are faraway (Zhang, Li & Wang 2004 and references therein). However, recently discovered Be/X-ray binary system with a black hole as the X-ray source (MWC 656; Casares et al. 2014) corroborates the model calculations. X-ray emitting compact object in most of the Be/X-ray binaries is generally a neutron star where as the optical companion is a B or O-type star that shows Balmer emission lines in its spectra. The neutron star in these binary systems is typically in a wide orbit with moderate eccentricity. The orbital period of these systems is in the range of 16-400 days.

X-ray emission in the Be/X-ray binary systems is known to be due to the accretion of mass from the Be circumstellar disk on to the neutron star at the periastron passage. The abrupt accretion of huge amount

of mass on to the neutron star results in strong X-ray outbursts (Okazaki & Negueruela 2001) enhancing the source luminosity by a factor of more than ~ 10 or more. Pulsars in these systems show periodic normal (Type I) X-ray outbursts that coincide with the periastron passage of the neutron star and giant (Type II) X-ray outbursts which do not show any clear orbital dependence (Negueruela et al. 1998). The spin period of these pulsars is found to be in the range of a few seconds to several hundred seconds. The X-ray spectra of these pulsars are generally hard. Fluorescent iron emission line at 6.4 keV is observed in the spectrum of most of the accretion powered X-ray pulsars. Cyclotron resonance scattering features (CRSF) have been detected in the broad-band X-ray spectrum of some of these pulsars. Detection of CRSF provides direct estimation of surface magnetic field of these objects. For a brief review of the properties of the transient Be/X-ray binary pulsars, refer to Paul & Naik (2011).

Transient Be/X-ray binary pulsar EXO 2030+375 was discovered during a giant outburst in 1985 with *EXOSAT* observatory (Parmar et al. 1989a). Optical and near-infrared observations identified a B0 Ve star as the counterpart of EXO 2030+375 (Motch & Janot-Pacheco 1987; Coe et al. 1988). Using the *EXOSAT* observation during the giant outburst, spin and orbital period of the binary pulsar were estimated to be 42 s and 44.3–48.6 days, respectively (Parmar et al. 1989a). During the declining phase of the giant outburst, the pulsar was found to be dramatically spinning-up at a timescale of $-P/\dot{P} \sim 30$ yr. Strong luminosity dependence of the pulse profile of EXO 2030+375 was detected during the giant outburst in 1985 (Parmar et al. 1989b). The pulse profile was characterized by the presence of two peaks which were separated by $\sim 180^\circ$ phase. The strength of the peaks in the pulse profile reversed as the pulsar luminosity decreased by a factor of ~ 100 . This was explained in terms of change in the pulsar emission from a fan-beam to a pencil-beam as the luminosity decreased resulting in the interchange in the strength of the main-pulse and inter-pulse. *Suzaku* observation of the pulsar at the peak of a Type I outburst, however, showed that the shape of pulse profiles was complex due to the presence of prominent dips at several pulse phases (Naik et al. 2013). The dips were found to be strongly energy dependent and were present up to as high as ~ 70 keV. An extensive monitoring of EXO 2030+375 with *BATSE* and Rossi X-ray Timing Explorer (*RXTE*) showed that a normal outburst has been detected for nearly every periastron passage for ~ 13.5 years (Wilson, Fabregat & Coburn 2005). Using *BATSE* observation of a series of consecutive Type I outbursts of the pulsar, Stollberg et al. (1997) derived the orbital parameters of the binary system.

The spectrum of the pulsar, obtained from *EXOSAT* observation during 1985 giant outburst was described by a composite model consisting of a blackbody component with temperature ~ 1.1 keV and a power law component describing the hard X-ray part (Reynolds, Parmar & White 1993; Sun et al. 1994). However, a model consisting of a blackbody and a power-law with an exponential cut-off was required to fit the 2.7–30 keV spectrum obtained from the *RXTE* observation of the pulsar during the 1996 June–July outburst (Reig & Coe 1999). Possible detection of cyclotron resonance scattering features at ~ 36 keV (Reig & Coe 1999), ~ 11 keV (Wilson et al. 2008), ~ 63 keV (Klochkov et al. 2008) in the spectrum of the pulsar have been reported earlier. However, the absence of any such feature in 1–100 keV spectrum of the pulsar ruled out the earlier suggestions of the detection of the cyclotron line in EXO 2030+375 (Naik et al. 2013). The broad-band *Suzaku* spectrum of the pulsar was best fitted with a partial covering high-energy cutoff power-law model. As the pulsar was very bright, several low-energy emission lines were also detected in the spectrum (Naik et al. 2013).

Suzaku observation of the pulsar at the peak of a Type I outburst of a significantly reduced intensity was used for a detailed study of the evolution and luminosity dependence of the absorption dips and corresponding changes in its spectral features. The results obtained from this study are described in this paper.

2 OBSERVATION

The transient Be/X-ray binary pulsar EXO 2030+375 shows bright Type I X-ray outbursts consistently at each periastron passage of the neutron star. The luminosity of the pulsar at the peak of these Type I outbursts are, however, found to be different. EXO 2030+375 was observed on 2007 May 14 and 2012 May 23 with the instruments onboard *Suzaku* when the pulsar was undergoing X-ray outbursts. During both the *Suzaku* observations, the peak luminosity was significantly different. One-day averaged light curve of EXO 2030+375 in 15–50 keV energy range obtained from the *Swift*/BAT monitoring data from 2006 November 21 to 2008 February 04 (top panel) and 2011 December 05 to 2013 March 09 (bottom panel)

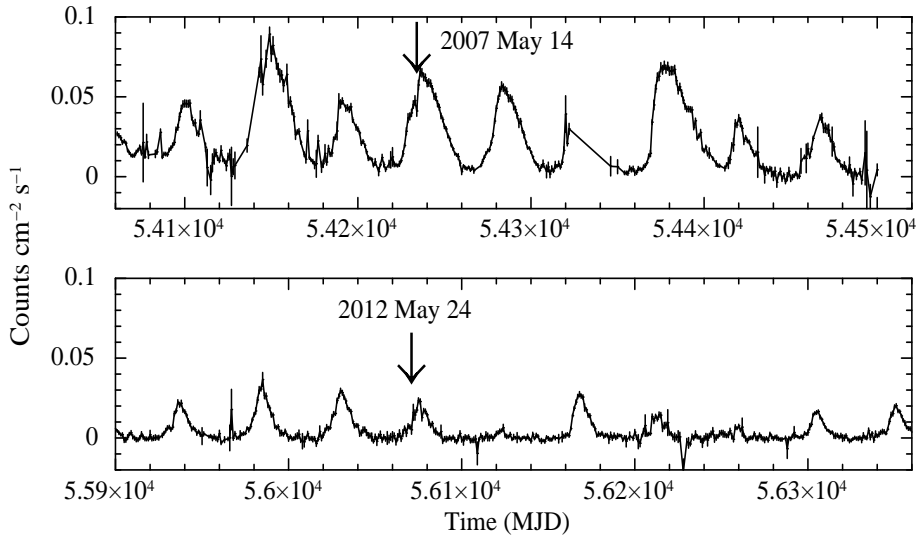


Fig. 1 *Swift*/BAT light curves of EXO 2030+375 in the 15-50 keV energy band, from 2006 November 21 (MJD 54060) to 2008 February 04 (MJD 54500) and 2011 December 05 (MJD 55900) to 2013 March 09 (MJD 56360) in top and bottom panels, respectively. The arrow marks in both the panels show the date of the *Suzaku* observations of the pulsar during its Type I outbursts.

covering both the Type I outbursts are shown in Figure 1. The arrow marks in both the panels show the *Suzaku* observations of the pulsar. The results obtained from the 2012 May *Suzaku* observation of the pulsar during a significantly less intense Type I outburst are discussed in this paper. The observation was carried out at the “XIS nominal” pointing position for a total exposures of ~ 78 ks and ~ 72.5 ks for the X-ray Imaging Spectrometer (XIS) and Hard X-ray Detector (HXD), respectively. The XIS was operated in the “1/4 window” option covering a $17'.8 \times 4'.4$ field of view.

Suzaku, the fifth Japanese X-ray astronomy satellite, was launched on 2005 July 10 (Mitsuda et al. 2007). It has two sets of detectors such as X-ray Imaging Spectrometer (XIS : Koyama et al. 2007) and Hard X-ray Detectors (HXD : Takahashi et al. 2007). Installed at the focal plane of four X-ray telescopes (XRT : Serlemitsos et al. 2007), the XIS consists of three front-illuminated CCD cameras (XIS-0, 2 & 3) and one back-illuminated CCD camera (XIS-1) sensitive in 0.4-12 keV and 0.2-12 keV energy ranges, respectively. The non-imaging instrument HXD acquires data in 10-70 keV range with the Si PIN photo diodes and in 40-600 keV range with the GSO scintillators. Combining XIS with HXD, *Suzaku* covers a broad energy band for the study of X-ray sources. The publicly available archival data (version 2.7.16.33) of the 2012 May observation of EXO 2030+375 were used in the present work. As XIS-2 was nonoperational during above observation of the pulsar, data from other three XIS, PIN and GSO were used in our analysis.

3 ANALYSIS AND RESULTS

We used HEASoft software package (version 6.12) in our analysis. The calibration database files released in 2012 February 10 (for XIS) and 2011 September 13 (for HXD) by the instrument teams are used for data reduction. The unfiltered XIS and HXD event data were reprocessed by using the “*aepipeline*” package of HEASoft. Barycentric correction was applied to the reprocessed XIS and HXD event data by using the “*aebarycen*” task of FTOOLS. These barycentric corrected XIS and HXD event files were used for further analysis. Source light curves and spectra were accumulated from the reprocessed XIS cleaned event data by selecting circular region with a $3'$ diameter around the central X-ray source. The background light curves and spectra were extracted from these event data by selecting circular regions away from the source position. “*xisrmfgen*” and “*xissimarfgen*” tasks were used to generate response files and effective area files

Table 1 Global spin period history of EXO 2030+375

| Date of Observation | MJD | Spin period | References |
|---|---------------|-----------------------|-----------------------|
| 1985 May 18 - 1985 Nov 03 ^a | 46203 - 46372 | 41.8327 s - 41.7275 s | Parmar et al. (1989a) |
| 1991-2003 ^b | 48400 - 52900 | 41.6910 s - 41.6736 s | Wilson et al. (2005) |
| 2006 June 22 - 2006 Nov 11 ^c | 53908 - 54050 | 41.6320 s - 41.4421 s | Wilson et al. (2008) |
| 2007 May 14 | 54234 | 41.4106 s | Naik et al. (2013) |
| 2012 May 24 | 56071 | 41.2852 s | present study |

^a : Maximum and minimum values of spin period out of 13 measurements (Table 1 of Parmar et al. 1989a), ^b : Maximum and minimum values of spin period out of 55 measurements (Figure 1 of Wilson et al. 2005), ^c : Maximum and minimum values of spin period out of 29 measurements (Figure 4, top panel of Wilson et al. 2008).

for corresponding XIS detectors. Hard X-ray light curves and spectra of the pulsar were extracted from the reprocessed HXD/PIN and HXD/GSO event data by using the “XSELECT” task of FTOOLS. Simulated background event data for HXD/PIN and HXD/GSO, provided by the instrument team were used to estimate background light curves and spectra for *Suzaku* observation of the pulsar. Response files released in 2011 June (for HXD/PIN) and 2010 May (for HXD/GSO) and an effective area file released on 2010 May for HXD/GSO were used for spectral analysis.

3.1 Timing Analysis

Source light curves with time resolutions of 2 s, 1 s and 1 s were extracted from the barycenter corrected XIS-0 (in 0.4-12 keV energy range), PIN (in 10-70 keV energy range) and GSO (in 40-200 keV energy range) event data, respectively. As described earlier, the background light curves were extracted for XIS, PIN and GSO detectors and subtracted from the source light curves. By applying pulse folding and χ^2 maximization technique, the spin period of the pulsar was estimated to be 41.2852(3) s. The estimated value of the pulse period of the pulsar showed a global spin-up trend while comparing with the earlier reported values. Earlier reported values of spin period of the pulsar at different epochs are tabulated in Table 1. Though spin-up, spin-down and constant spin frequency episodes are observed at smaller time scales (Parmar et al. 1989a; Wilson et al. 2005; 2008), the pulsar showed overall spin-up trend at longer time scale.

The pulse profiles of the pulsar were obtained by folding the background subtracted light curves obtained from XIS, PIN and GSO data with the estimated spin period and are shown in Figure 2. It can be seen from this figure that the pulse profiles are significantly different at different energy ranges. The shape of the pulse profiles obtained from the 2012 May *Suzaku* observation of the pulsar was found to be significantly different to that reported from earlier observations (Naik et al. 2013 and references therein). A single-peaked profile in 0.4-12 keV range (top panel) changed to a structured double-peaked profile in 10-70 keV range (middle panel) which again became smooth and single-peaked in 40-200 keV range (bottom panel).

To investigate the evolution of the pulse profile with energy, light curves at various energy ranges were extracted from the XIS, PIN and GSO event data. Background light curves in same energy ranges were also extracted and subtracted from the corresponding source light curves. Energy resolved pulse profiles were generated by using the estimated spin period of the pulsar and shown in Figure 3. It can be seen that the pulse profile of the pulsar was single-peaked up to ~ 8 keV beyond which a hump-like structure appeared after the main peak. The pulse profile became double-peaked up to ~ 40 keV beyond which it again became single-peaked. The 41.2852 s pulsation was seen in HXD/PIN and HXD/GSO light curves up to ~ 70 keV range, beyond which it was absent. Though energy dependent pulse profiles are seen in EXO 2030+375, the profiles obtained during the 2012 May outburst are significantly different to that obtained during 2007 May outburst. Though the observations were carried out during Type I outbursts with the detectors onboard *Suzaku*, entirely different type of pulse profiles require a detailed spectral investigation to understand the emission mechanism in the pulsar.

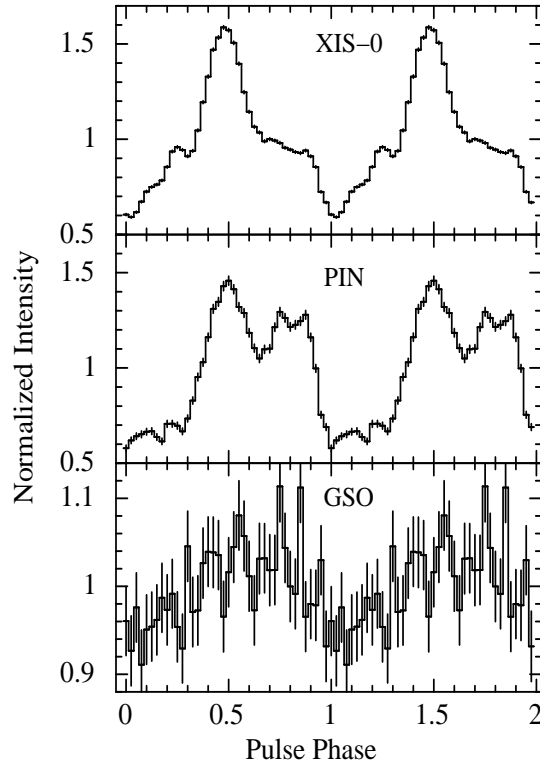


Fig. 2 Pulse profiles of EXO 2030+375 in 0.4–12 keV range (XIS-0; top panel), 10–70 keV range (PIN; middle panel) and 40–200 keV range (GSO; bottom panel), obtained from the background subtracted light curves by using the estimated 41.2852 s pulse period. The errors in the figure are estimated for the 1σ confidence level. Two pulses are shown for clarity.

3.2 Spectral Analysis

3.2.1 Pulse-phase-averaged spectroscopy

We carried out simultaneous spectral fitting of the XIS (XIS-0, XIS-1 and XIS-3), PIN and GSO data to investigate the energy dependence of pulse profile seen in 2012 May *Suzaku* observation of EXO 2030+375. As described earlier, source spectra were extracted from the XIS, PIN and GSO event data and corresponding background spectra and response files were obtained by following appropriate procedure. Using the extracted source spectra, background spectra and response files, simultaneous spectral fitting was carried out using the software package XSPEC v12.7.1. Because of the presence of known structures in the XIS spectra at Si and Au edge, data in the 1.7–1.9 keV and 2.2–2.4 keV range were ignored from the spectral fitting. XIS spectra were re-binned by a factor of 6 from 1 to 10 keV whereas the HXD/PIN spectrum was re-binned by a factor of 4 from 23 keV to 45 keV and by a factor of 6 from 45 keV to 70 keV. The binning of GSO spectrum, however, was done as suggested by the instrument team¹. In the spectral fitting, all the model parameters were tied together except for the relative instrument normalizations. The broad-band energy spectra in 1–100 keV energy range were fitted with several continuum models such as (i) high-energy cutoff power-law model, (ii) a power-law with high energy exponential rolloff, and (iii) Negative and Positive power law with EXponential cutoff (NPEX) continuum model. The analytical form of above continuum models are

¹ <http://heasarc.gsfc.nasa.gov/docs/suzaku/analysis/gsobgd64bins.dat>

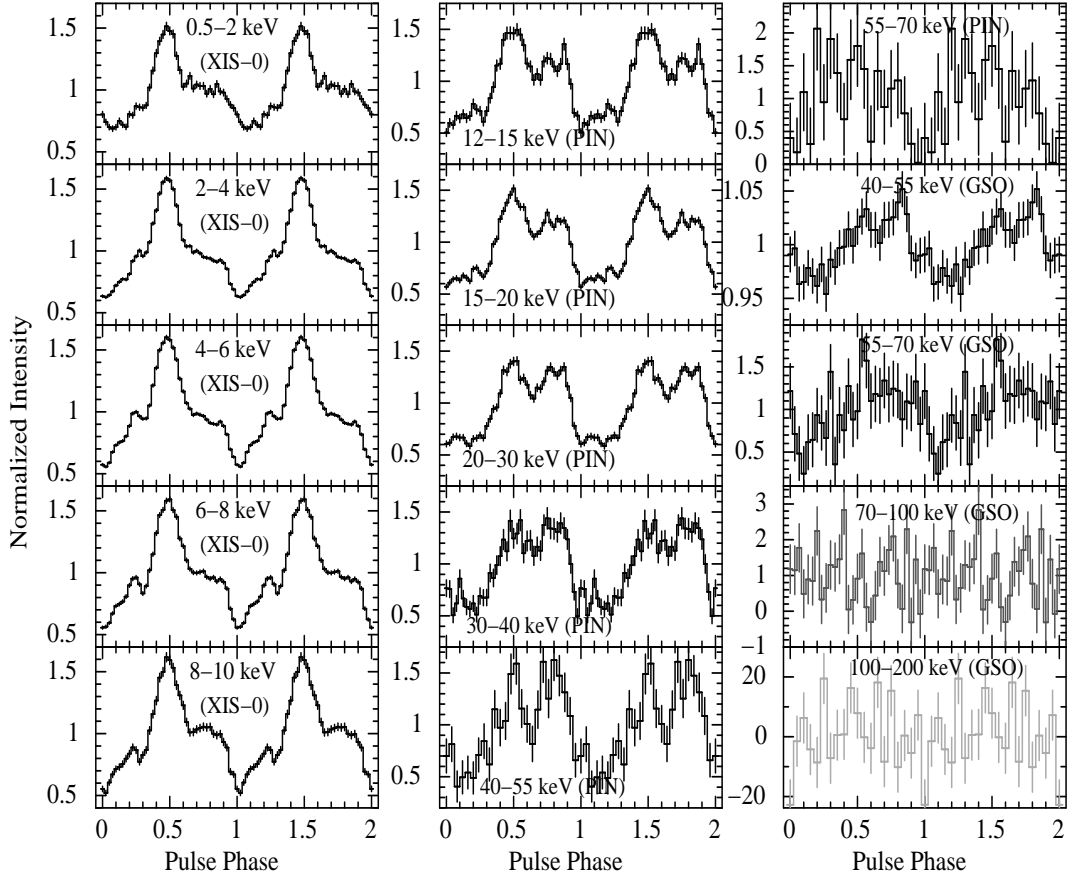


Fig. 3 Energy-resolved pulse profiles of EXO 2030+375 obtained from XIS-0, HXD/PIN and HXD/GSO light curves at various energy ranges. The presence of absorption dips in profiles at higher energies can be seen in 0.6–0.8 pulse phase range. The error bars represent 1σ uncertainties. Two pulses in each panel are shown for clarity.

High energy cutoff power law model -

$$I(E) = \begin{cases} E^{-\gamma} & (E \leq E_c) \\ E^{-\gamma} \exp\left(-\frac{E-E_c}{E_f}\right) & (E > E_c) \end{cases} \quad (1)$$

where E_c and E_f are cutoff energy and folding energy, respectively.

High energy exponential rolloff model -

$$I(E) = K E^{-\alpha} e^{-E/kT} \quad (2)$$

where, K is normalization constant and α is photon index. kT represents cutoff-energy of power-law in unit of keV.

NPEX continuum model -

$$NPEX(E) = (N_1 E^{-\alpha_1} + N_2 E^{+\alpha_2}) e^{-E/kT} \quad (3)$$

Table 2 Best-fit parameters (with 1σ errors) obtained from the spectral fitting of the 1-100 keV spectra of the *Suzaku* observation of EXO 2030+375 during the 2012 May Type I outburst. Model-I, Model-II and Model-III represent the partially absorbed power law with a high-energy cutoff continuum model with interstellar absorption and Gaussian components, a partially absorbed power law with high-energy exponential rolloff model with interstellar absorption and Gaussian components and a partially absorbed NPEX continuum model with interstellar absorption and Gaussian components, respectively.

| Parameter | Value | | |
|---|-------------------------|-------------------------|-------------------------|
| | Model-I | Model-II | Model-III |
| N_{H1} (10^{22} atoms cm^{-2}) | 2.02 ± 0.02 | 2.02 ± 0.02 | 1.93 ± 0.02 |
| N_{H2} (10^{22} atoms cm^{-2}) | 4.47 ± 0.15 | 5.16 ± 0.15 | 4.70 ± 0.17 |
| Covering fraction | 0.53 ± 0.01 | 0.50 ± 0.01 | 0.44 ± 0.01 |
| High energy cut-off (keV) | 6.52 ± 0.13 | 20.2 ± 0.4 | 10.6 ± 0.6 |
| E-fold energy (keV) | 24.6 ± 0.5 | — | — |
| Power-law index | 1.26 ± 0.01 | 1.07 ± 0.01 | 0.79 ± 0.04 |
| Iron line energy (keV) | 6.41 ± 0.01 | 6.42 ± 0.01 | 6.42 ± 0.01 |
| Iron line width (keV) | 0.01 ± 0.01 | 0.03 ± 0.01 | 0.03 ± 0.01 |
| Iron line equivalent width (eV) | 27 ± 2 | 33 ± 2 | 33 ± 2 |
| 1-10 keV flux ^a | 4.5 ± 0.2 | 4.6 ± 0.1 | 4.6 ± 0.2 |
| 10-70 keV flux ^a | 10.6 ± 0.3 | 10.3 ± 0.2 | 10.6 ± 1.4 |
| Reduced χ^2 | 1.36 (650 dof) | 1.41 (651 dof) | 1.38 (650 dof) |
| Relative Inst. Normalization (XIS-0/XIS-1/XIS-3/PIN/GSO) | 1.0/0.94/0.99/1.11/1.06 | 1.0/0.94/0.99/1.04/1.11 | 1.0/0.94/0.99/1.11/1.09 |

N_{H1} = Equivalent hydrogen column density, N_{H2} = additional hydrogen column density, ^a : in 10^{-10} ergs cm^{-2} s $^{-1}$ unit. Quoted source flux is not corrected for interstellar absorption.

where E is energy of X-ray photons, N_1 , N_2 , α_1 , α_2 are normalization and index of negative and positive power-law, respectively. kT represents cutoff-energy of power-law in unit of keV.

Additional components such as photoelectric absorption, a Gaussian function for an iron emission line were added to the continuum models while fitting the pulsar spectra. It was found that all the continuum models provided similar fits to the pulsar spectra with reduced χ^2 of ~ 1.7 . As in case of other Be/X-ray binary pulsars, a partial covering absorption component *pcfabs* was then applied to above continuum models in the spectral fitting. Addition of this component to above three continuum models improved the spectral fitting significantly yielding a reduced χ^2 of ~ 1.4 . The best-fit parameters obtained from the simultaneous spectral fitting to the XIS, PIN and GSO data are given in Table 2. The count rate spectra of the pulsar EXO 2030+375 are shown in Figure 4 (for high-energy cutoff power-law model), Figure 5 (for power-law with high energy exponential rolloff model), and Figure 6 (for NPEX continuum model) along with the model components (top panels) and residuals to the fitted models (bottom panels). In the spectral fitting using above models, there was no signature of presence of a cyclotron resonance scattering feature (CRSF) at earlier reported energies in EXO 2030+375.

3.2.2 Pulse-phase-resolved spectroscopy

Accretion powered transient X-ray pulsars show complex pulse profiles in soft X-ray bands that gradually become smooth and single-peaked at higher energies. As the soft X-ray photons emitted from the polar caps of the pulsar are generally most affected due to the absorption by matter distributed in the vicinity of the neutron star and in the interstellar medium, the shape of the pulse profiles become complex which is not the case in higher energies. However, the shape of the pulse profiles of EXO 2030+375 obtained from the 2012 May *Suzaku* observation is rather smooth and single-peaked at soft X-rays and complex in higher energies. Therefore, it is interesting to do a detailed spectral study at narrow pulse phases of the transient pulsar during the 2012 May outburst. For the pulse phase resolved spectral study, we used data from XIS (XIS-0, XIS-1 & XIS-3) and HXD/PIN detectors. We did not include HXD/GSO data in phase-resolved spectroscopy because of the lack of sufficient number of photons at each phase bin of the pulsar. XIS

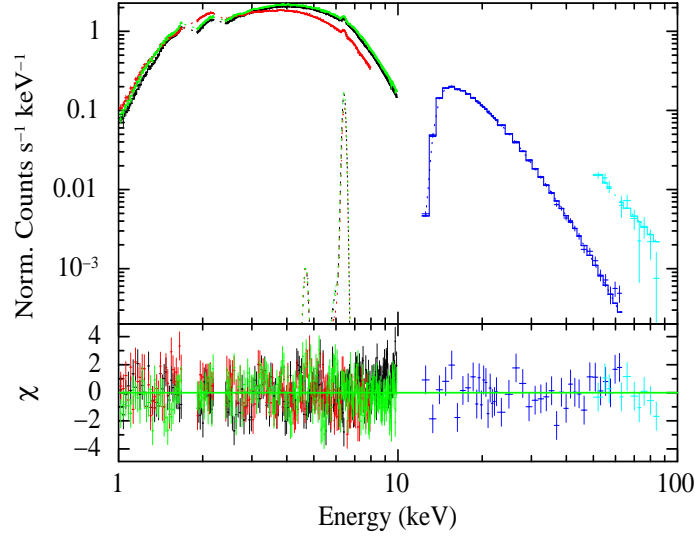


Fig. 4 Energy spectrum of EXO 2030+375 obtained with the XIS-0, XIS-1, XIS-3, PIN, and GSO detectors of the *Suzaku* observation during the 2012 May-June Type I outburst, along with the best-fit model comprising a partially absorbed power law with a high-energy cutoff power law continuum model, a Gaussian function for the narrow iron emission line along with the interstellar absorption. The contributions of the residuals to the χ^2 for each energy bin for the best-fit model are shown in the bottom panel.

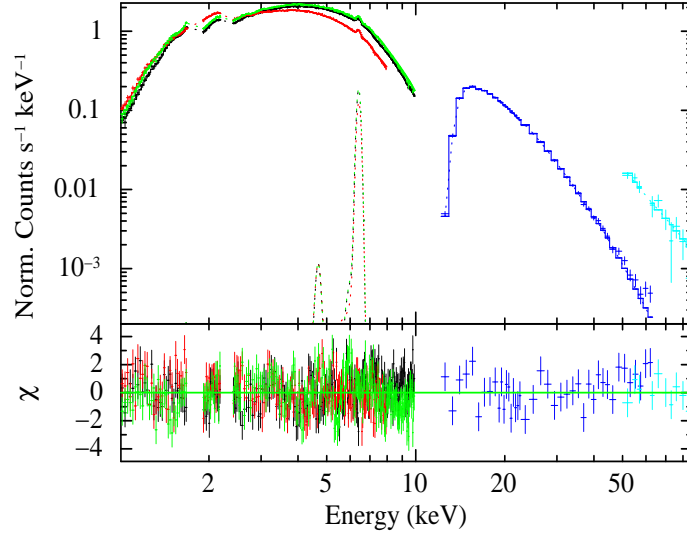


Fig. 5 Energy spectrum of EXO 2030+375 obtained with the XIS-0, XIS-1, XIS-3, PIN, and GSO detectors of the *Suzaku* observation during the 2012 May-June Type I outburst, along with the best-fit model comprising a partially absorbed power law with high-energy exponential rolloff model, a Gaussian function for the narrow iron emission line along with the interstellar absorption. The contributions of the residuals to the χ^2 for each energy bin for the best-fit model are shown in the bottom panel.

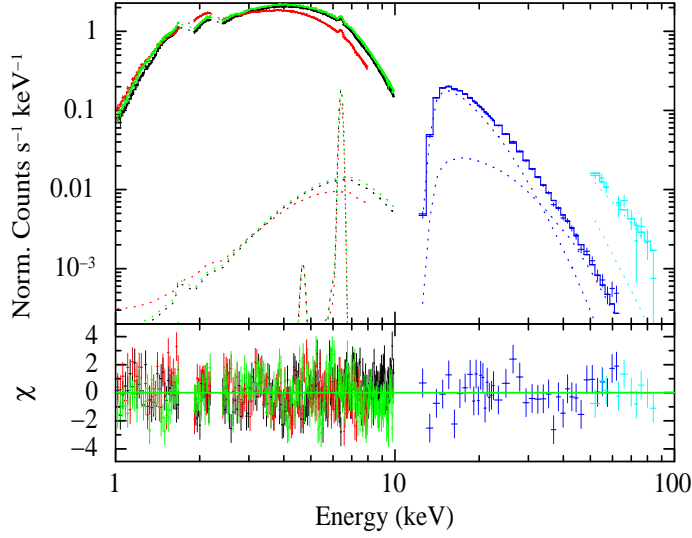


Fig. 6 Energy spectrum of EXO 2030+375 obtained with the XIS-0, XIS-1, XIS-3, PIN and GSO detectors of the *Suzaku* observation during the 2012 May-June Type I X-ray outburst. The data are plotted with the best-fit model comprising a partially absorbed NPEX continuum model and a Gaussian function for the narrow iron emission line along with the interstellar absorption. The contributions of the residuals to the χ^2 for each energy bin for the best-fit model are shown in the bottom panel.

and PIN spectra were accumulated into 20 pulse-phase bins by applying phase filter in the FTOOLS task XSELECT. Background spectra, response matrices used in the phase-averaged spectroscopy were also used in the phase-resolved spectral analysis. As all three continuum models were yielding similar results while fitting phase-averaged spectra, two of the three models (high-energy cutoff power-law and NPEX continuum models) were used for simultaneous spectral fitting to the phase-resolved spectra in 1-70 keV range. In the spectral fitting, the values of relative instrument normalizations were fixed at the values obtained from the phase-averaged spectroscopy (as given in Table 2). It was found that certain parameters such as absorption column density (N_{H1}), iron line energy and line width did not show any significant variation over pulse phases of the pulsar. Therefore, these parameters were also fixed at the phase-averaged values.

Parameters obtained from the simultaneous spectral fitting to the phase-resolved XIS and PIN data in 1-70 keV range are shown in Figure 7. Pulse profiles obtained from XIS and PIN data are shown in top two panels on both the sides of the figure. Parameters obtained from the spectral fitting using partially absorbed NPEX and high-energy cutoff power-law continuum models along with interstellar absorption and Gaussian function are shown in left and right panels of the figure, respectively. It can be seen that the parameters obtained from the phase-resolved spectral fitting using two different continuum models followed similar pattern over pulse phases of the pulsar. In case of both the models, the value of additional column density (N_{H2}) was found to be high in 0.6-0.9 pulse phase range. High value of additional column density can explain the absence of significant amount of soft X-ray photons in above pulse phase range. The absorption of soft X-ray photons by the additional matter makes the pulse profile shallow in 0.6-0.9 pulse phase range (top panels of Figure 7). However, at hard X-rays, the effect of the additional matter is drastically reduced making the pulse profile different compared to that in soft X-ray bands. The pulsar spectrum was found to be marginally hard in 0.8-1.1 phase range along with high value of cutoff energy and iron line equivalent width. This coincides with the presence of a dip (primary dip in the pulse profile) in the pulse profile at this phase range.

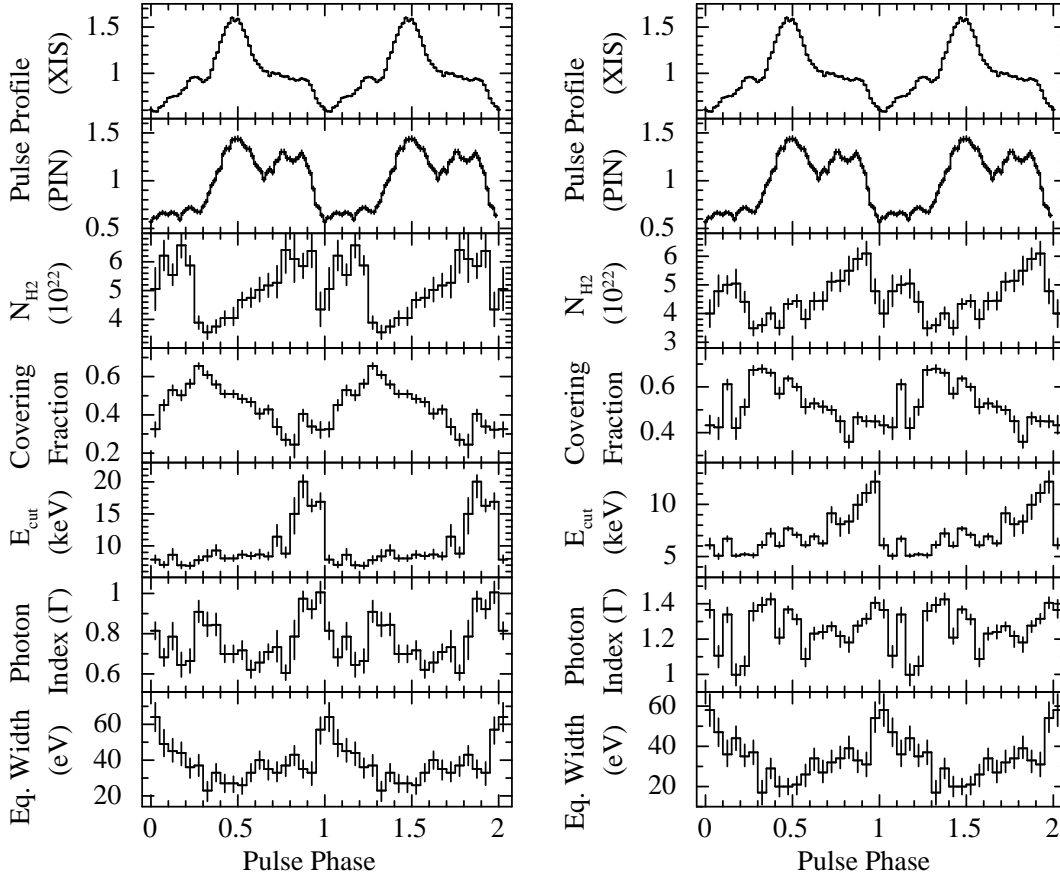


Fig. 7 Spectral parameters obtained from the pulse-phase-resolved spectroscopy of *Suzaku* observation of EXO 2030+375. The XIS (in 0.4–12 keV range) and PIN (in 10–70 keV range) pulse profiles are shown in top two panels of both sides of the figure, respectively. The other panels show the spectral parameters obtained by using a partial covering NPEX continuum model (left panels) and a partial covering cutoff power law continuum model (right panels). The errors shown in the figure are estimated for 1σ confidence level.

4 DISCUSSION

The timing and spectral properties of transient Be/X-ray pulsar EXO 2030+375 have been reported earlier (Naik et al. 2013 and references therein). During normal Type I outbursts, the pulse profile of the pulsar was found to be strongly energy and luminosity dependent. At high luminosity, the pulse profile of the pulsar was found to be complex because of the presence of several narrow prominent dips at various spin phases (Naik et al. 2013). At low luminosity level, however, the pulse profile was smooth and single-peaked (Parmar et al. 1989). Strong luminosity dependence of the pulse profile in EXO 2030+375 has been reported earlier by using observations from several observatories (as discussed in Naik et al. 2013 and references therein). Though the pulsar was observed with *Suzaku* during two Type I outbursts, the shape of the profiles obtained from these observations were significantly different. During 2007 May Type I outburst, the shape of the pulse profile was complex due to the presence of several energy dependent narrow dips at various pulse phases. The strength of these dips gradually decreased with increase in energy, making the hard X-ray profile smooth and single-peaked. However, during the 2012 May Type I outburst, the shape of the profile was entirely different – a narrow single-peaked profile at soft X-rays which became a double-peaked

profile up to ~ 55 keV beyond which it again became single-peaked. Investigation of significant difference in the shape of pulse profiles during 2007 May and 2012 May Type I outbursts may provide information regarding the geometry of the matter distribution around the poles of the neutron star. Accretion of huge amount of matter onto the neutron star (during bright X-ray outbursts in Be/X-ray binary pulsars) causes changes in the geometry of the matter distribution around the neutron star from a smooth accretion stream to several narrow accretion streams that are phase-locked with the neutron star. These narrow streams of matter causes several absorption dips in the pulse profiles during bright X-ray outbursts. However, during low mass accretion duration, the observed pulse profiles are relatively smooth which is seen in case of 2012 May observation of EXO 2030+375 compared to that during 2007 May outburst.

During 2007 May *Suzaku* observation, the pulsar was bright in X-ray compared to that during 2012 May observation. The source flux in 1-70 keV range was estimated to be $\sim 8.9 \times 10^{-9}$ erg cm $^{-2}$ s $^{-1}$ (Naik et al. 2013). However, during the 2012 May observation, the pulsar was much fainter with estimated 1-70 keV flux of $\sim 1.5 \times 10^{-9}$ erg cm $^{-2}$ s $^{-1}$ (present work). It was also evident from Figure 1 that the 2007 May Type I outburst was much brighter in 15-50 keV range compared to the 2012 May Type I outburst. While comparing spectral properties of the pulsar, it was found that partial covering absorption model fitted well to the broad-band *Suzaku* spectra during both the observations. The value of absorption column density (N_{H1}) obtained from the spectral fitting was found to be comparable in both the cases. However, the value of additional absorption column density (N_{H2}) was about an order of magnitude higher during 2007 May observation compared to that during 2012 May observation. As the pulsar was bright during 2007 May observation, several narrow emission lines were also detected in the spectrum. Significantly high value of additional absorption column density and presence of several narrow and prominent absorption dips in the pulse profiles during the high luminosity level of the pulsar indicate the accretion of huge amount of mass from the circumstellar disk of Be companion star during 2007 May outburst. Pulse-phase resolved spectroscopy of 2007 May *Suzaku* observation revealed the presence of narrow streams of matter causing the absorption dips in the pulse profile and are phase locked with the pulsar. Lower value of additional column density, absence of absorption dips in the pulse profile of the pulsar and about an order of magnitude less luminous during 2012 May *Suzaku* observation confirm that mass accretion from the circumstellar disk of the Be star to the neutron star was significantly low compared to that during 2007 May observation.

In case Be/X-ray binary pulsars, it is known that the observed regular and periodic X-ray outbursts during the periastron passage of the neutron star are due to the evacuation of matter from the circumstellar disk of the Be star. Regular monitoring of these Be/X-ray binary pulsars showed that the peak luminosity of the neutron star during these outbursts varies with time e.g. in case of EXO 2030+375, peak luminosity of the pulsar varies by an order of magnitude between the 2007 May and 2012 May X-ray outbursts. The change in the peak luminosity during the outbursts can be explained as due to the difference in the amount of mass evacuated from the Be circumstellar disk by the neutron star during the periastron passage which in turn depends on the evolution of the Be circumstellar disk. Therefore, we suggest that the size of the circumstellar disk of the Be star in EXO 2030+375 binary system was relatively small during the 2012 May outburst compared to that during 2007 May observation.

Presence of dips in the pulse profile are seen in many transient Be/X-ray binary pulsars such as A 0535+262 (Naik et al. 2008), GRO J1008-57 (Naik et al. 2011), 1A 1118-61 (Maitra et al. 2012) etc. The evolution of pulse profiles of Be/X-ray binary pulsars from a smooth single-peaked profile (during quiescence) to a complex shape because of the presence of several prominent absorption dips (during Type I outbursts) are briefly described in Paul & Naik (2011) and Naik (2013) and references therein. Presence of the absorption dips in the pulse profiles of these transient Be/X-ray binary pulsars is explained as due to the abrupt accretion of huge amount of matter that disrupts the accretion stream into several narrow streams of matter that are phase locked with the neutron star. The presence of dips in the pulse profiles of Be/X-ray transient pulsars during Type I outbursts can be compared with the effect of abrupt mass accretion onto weakly magnetized stars. Three-dimensional Magnetohydrodynamic (MHD) simulations of mass accretion from the companion to weakly magnetized stars such as weakly magnetized neutron stars (millisecond pulsar), magnetized white dwarfs in some cataclysmic variables etc. showed that during unstable regime of mass accretion, the accreted matter can penetrate into the magnetosphere leading to stochastic light curves (complex pulse profiles) whereas in stable accretion regime, matter gets accreted in the form of streams yielding almost periodic light curves (Romanova et al. 2008). In case of Be/X-ray binary pulsars, signif-

ificant amount of mass is being accreted onto the neutron star at the periastron passage, leading to X-ray outbursts. Depending on the amount of mass evacuated from the circumstellar disk of the Be star, the pulse profile of the Be/X-ray binary pulsar gets modified as seen in case of EXO 2030+375 – a complex profile because of the presence of several narrow and prominent dips at high luminosity level and a relatively smooth profile at low luminosity level. Therefore, the change in shape of the pulse profiles with luminosity in Be/X-ray binary pulsars agrees with the theoretical prediction by Romanova et al. (2008) though it was done for low magnetic objects.

ACKNOWLEDGMENTS

We thank the anonymous referee for his/her useful suggestions that improved the manuscript. The research work at Physical Research Laboratory is funded by the Department of Space, Government of India. The authors would like to thank all the members of the *Suzaku* for their contributions in the instrument preparation, spacecraft operation, software development and in-orbit instrumental calibration. This research has made use of data obtained through HEASARC Online Service, provided by the NASA/GSFC, in support of NASA High Energy Astrophysics Programs.

References

- Casares, J., Negueruela, I., Ribó, M., Ribas, I., Paredes, J. M., Herrero, A., Simón-Díaz, S., 2014, *Nature*, 505, 378
- Coe, M. J., Longmore, A., Payne, B. J., Hanson, C. G., 1988, *MNRAS*, 232, 865
- Klochkov, D., Santangelo, A., Staubert, R., Ferrigno, C., 2008, *A&A*, 491, 833
- Koyama, K., Tsunemi, H., Dotani, T., et al. 2007, *PASJ*, 59S, 23
- Maitra, C., Paul, B., Naik, S., 2012, *MNRAS*, 420, 2307
- Mitsuda, K., Bautz, M., Inoue, H., et al. 2007, *PASJ*, 59S, 1
- Motch, C., Janot-Pacheco, E., 1987, *A&A*, 182, L55
- Naik, S., 2013, *ASI Conf. Ser.*, 8, 103
- Naik, S., Dotani, T., Terada, Y., et al. 2008, *ApJ*, 672, 516
- Naik, S., Paul, B., Kachhara, C., Vadawale, S. V., 2011, *MNRAS*, 413, 241
- Naik, S., Maitra, C., Jaisawal, G. K., & Paul, B., 2013, *ApJ*, 764, 158
- Negueruela, I., Reig, P., Coe, M. J., & Fabregat, J., 1998, *A&A*, 336, 251
- Okazaki, A. T., Negueruela, I., 2001, *A&A*, 377, 161
- Parmar, A. N., White, N. E., Stella, L., Izzo, C., Ferri, P., 1989a, *ApJ*, 338, 359
- Parmar, A. N., White, N. E., Stella, L., 1989b, *ApJ*, 338, 373
- Paul, B., Naik, S., 2011, *BASI*, 39, 429
- Reig, P., Coe, M. J., 1999, *MNRAS*, 302, 700
- Reynolds, A. P., Parmar, A. N., White, N. E., 1993, *ApJ*, 414, 302
- Romanova, M. M., Kulkarni, A. K., & Lovelace, R. V. E., 2008, *ApJL*, 673, 171
- Serlemitsos, P. J., et al. 2007, *PASJ*, 59, S9
- Stollberg, M. T., 1997, PhD thesis, Univ. Alabama
- Sun, X.-J., Li, T.-P., Wu, M., Cheng, L.-X., 1994, *A&A*, 289, 127
- Takahashi, T., Abe, K., Endo, M., et al. 2007, *PASJ*, 59S, 35
- Wilson, C. A., Fabregat, J., Coburn, W., 2005, *ApJ*, 620, L99
- Wilson, C. A., Finger, M. H., Camero-Arranz, A., 2008, *ApJ*, 678, 1263
- Zhang, F., Li, X.-D., Wang, Z.-R., 2004, *ApJ*, 603, 663